Available online at www.sciencedirect.com
SCIENCE DIRECT®
Journal of Computational Physics 205 (2005) 686–705
JOURNAL OF COMPUTATIONAL PHYSICS
www.elsevier.com/locate/jcp

An efficient model for three-dimensional surface wave simulations. Part II: Generation and absorption

Didier Clamond, Dorian Fructus, John Grue *, Øyvind Kristiansen

Mechanics Division, Department of Mathematics, University of Oslo, P.O. Box 1053, Blindern, 0316 Oslo, Norway

Received 1 July 2004; received in revised form 25 November 2004; accepted 25 November 2004
Available online 25 February 2005

Abstract

Water wave generation procedures and efficient numerical beaches are crucial components of a fully non-linear numerical tank for water wave simulations. Linear formulae for pneumatic wave makers are optimized for efficient fully non-linear wave generation in three dimensions. Analytical integration of the (linear) applied free surface pressure provides formulae valid for all times of the simulation. The purely non-linear part of the wave making procedure becomes integrated in the fully non-linear formulation. Novel numerical beaches are introduced, damping the (scaled) tangential velocity at the free surface. More specifically, an additional term is introduced in the Bernoulli equation at the free surface, namely $\nabla^{-1}\cdot(\gamma\nabla\tilde{\phi})$, where γ is a non-zero (smooth) function in regions where damping is required and zero in the wave propagation domain, $\nabla\tilde{\phi}$ is the scaled tangential velocity at the free surface, and ∇^{-1} the inverse horizontal gradient operator. The new term results in a modified dynamic free surface condition which is integrated in time in the fully non-linear formulation. Extensive numerical tests show that the energy of the outgoing waves is completely absorbed by the new damper. Neither wave reflection nor emission are observed. A steep solitary wave is completely absorbed at the numerical beach. Damping of waves due to advancing pressure distributions are efficient as well. The implementation of the absorber in any existing numerical tank is rather trivial.

Keywords: Surface waves; Non-linear wave generation; Pneumatic wave makers; Absorbing boundary conditions; Integral equations, Laplace equation

* Corresponding author. Tel.: +47 2285 5839; fax: +47 2285 4349.
E-mail addresses: didier@math.uio.no (D. Clamond), dorianf@math.uio.no (D. Fructus), johng@math.uio.no (J. Grue), oyvinkri@math.uio.no (Ø. Kristiansen).

0021-9991/$ - see front matter
doi:10.1016/j.jcp.2004.11.038

1. Introduction

Despite intensive investigations by the scientific and engineering communities for about two centuries, many aspects of surface wave dynamics are far from understood. Experimental campaigns play a crucial role in the discovery and understanding of the phenomenae. Indeed, experiments are used to validate theories, test the design of offshore structures at laboratory scale, and to discover new features of the waves. Many of the experiments require quite large facilities which are expensive to build and maintain, however. A cheaper possibility consists in using numerical modelling. The numerical resolution of the equations governing surface waves is a non-trivial task. This is due to their non-linearity and the fact that the computational domain is unknown since the free surface evolves in time. In a companion paper, Fructus et al. [7] a fast and accurate numerical method for direct simulations of fully non-linear surface waves in three-dimensions was presented. The method was outlined for periodic free space problems, meaning that the evolution of the total (periodic) wave field is studied, given the wave field at an initial time. Realistic simulations of experiments require generation of wave fields from rest, however. Further, the problems are not always spacially periodic.

In this paper, novel procedures are derived for wave generation and wave absorption, including also a complete description of their numerical implementation and use in practice, extending the periodic wave tank explained in [7] (Part I of the paper). The hypotheses and notations used here are identical to those used in Part I. For an easy reference, they are briefly given in Section 2 of this paper. An accurate wave generation procedure involves all the steps from a rigorous linear wave analysis to an integrated, fully non-linear procedure. These are steps that require a thorough analysis and is the motivation for the derivations that are made here. Equally important is to communicate the mathematical and physical justifications of a novel fully non-linear wave damping procedure. While the theoretical deductions and considerations are of value in itself, their ultimate performance is illustrated in real simulations of steep water waves. The relevant method for such tests is the complementary rapid, fully non-linear wave simulator in 3D, derived in the accompanying paper, Part I. We shall see with the tests that the highly non-linear wave generation procedure is easily controlled. With regards to wave damping, the accurate three-dimensional simulations show that there is practically speaking a perfect absorption of the out-going non-linear waves and the associated energy at an arbitrary boundary of the computational domain. The generation and absorption procedures are the novel contributions in this paper.

To generate waves from rest we use pneumatic wave makers. We prescribe a pressure distribution at the surface that is localized in space and evolves in time. The method is easy to adapt and implement with an Eulerian description of the motion. This is the case for the present model. To be efficient, a wave maker must transmit as much energy as possible to the far field, meaning that the pneumatic wave maker cannot be chosen completely arbitrarily. The exact theory of wave generation is untractable, but the linear theory of pneumatic wave making is well established (see, Wehausen and Laitone [13, Section 21]). The linear theory allows us to optimize the wave makers. To our knowledge, the validity of this optimization is less tested in fully non-linear simulations. Formulae for three types of pneumatic generators are described in detail and implemented numerically: (i) a purely oscillating long-crested (two-dimensional) wave generator; (ii) a purely oscillating axisymmetric wave generator; (iii) a moving at constant speed non-oscillating pressure distribution, see Section 3. Many other pneumatic wave makers may as well be defined and optimized along the same lines. The examples given in this paper are general and sufficiently successful, making us believe that other pneumatic wave makers will be efficient as well.

Other methods for generating waves may also be considered. Piston wave makers and plunger wave makers are widely used in experimental facilities, for example. Their linear theory is well established [6]. These methods are less well suited than a pneumatic generation in fully non-linear simulations, however. Indeed, to model paddle wave makers one has to treat carefully the singularity at the intersection between the free surface and the paddle. That is a non-trivial task. Moreover, paddle wave makers impose condi-

tions on the particle displacements that are difficult to treat properly within an Eulerian model, as the one we develop. Such problems do not arise with a pneumatic wave maker which allows a sudden temporal variation in its motion without numerical difficulties.

Simulations of non-periodic problems extending to infinity in the horizontal directions require artificial truncation of the computational domain. An efficient absorption of outgoing waves at the truncation boundary is therefore crucial. For linear problems, the technique of analytical radiation conditions provide efficient representation of the waves in the far field. This technique can be extended to include weakly non-linear perturbation formulations, but looses its power in the case of strongly non-linear problems. Alternative strategies using so-called *open boundary conditions* have long been discussed, see, e.g., Givoli [9] and Romate [12]. Recent developments of non-reflecting boundary conditions include, e.g., works by Alpert et al. [1], Givoli [10]. While the former paper focuses on applications to the usual wave equation, exploring a new technique for efficiently applying the exact non-reflecting boundary conditions, the authors conclude that the method is not capable for treatment of wave propagation in infinite layered media, like wave propagation in a deep ocean. The other paper reviews high-order non-reflecting boundary conditions. Damping at the numerical truncation boundary of model equations like the two-dimensional wave equation and the Klein-Gordon equation are discussed.

One of the classical sponge layer techniques consists in modifying the surface dynamic condition, i.e., the Bernoulli equation, for example. A term proportional to the velocity potential is added to the equation. The term is non-zero where damping is required. If the sponge layer is too short or too strong, waves are not completely absorbed when they encounter the damping layer. We have tested several classical numerical damping beaches, finding that their applicability is rather limited, causing severe wave reflection and even wave emission at the boundaries.

In Section 4, we give reasons for the non-effectiveness of the classical sponge layer technique. The considerations lead to a natural modification of the damping method, as we develop a new open boundary condition. The novel step is to damp the (scaled) tangential velocity at the free surface. More specifically, an additional term is introduced in the Bernoulli equation at the free surface. This new absorber is physically more consistent and more effective than previous techniques. The modified damper is easy to implement and efficient, whatever the geometry of the open boundary is. Moreover, all the frequencies are equally damped and the absorber can be short and strong without parasitic effects. The efficiency is demonstrated via several examples in Section 5.

While the velocity field is damped by the new term in the free surface dynamic boundary condition, and the mass not, a wave induced mass transport may also be absorbed. For this purpose another modification is introduced: now a damping term proportional to the free surface elevation is added in the free surface kinematic boundary condition [2,3], see Section 4.3. A solitary wave leaving the computational domain represents an example in this respect. The new method completely absorbs the solitary wave.

The method for wave generation and absorption is tested in Section 5, using the fully non-linear model described in Part I (Fructus et al. [7]). We consider domains with simple and complex geometries encapsulated by rectangular computational boxes. Simulations are performed in deep water, intermediate water depth and in shallow water, for various types of waves. The broad effectiveness of the pneumatic generation and of the new absorbing boundary condition, as well as the efficiency of the numerical model, in complement to the tests performed in Part I, is demonstrated.

2. Mathematical formulation

We consider three-dimensional irrotational wave motions at the surface of a homogeneous incompressible fluid over a horizontal impermeable bottom. The resulting equations and their numerical resolution are detailed in Part I. For an easy reference, the notations and the equations are briefly presented below.

Let $\boldsymbol{x} = (x_1, x_2)$, y and t be, respectively, the horizontal Cartesian coordinates, the upward vertical one and the time. $y = 0$, $y = -h$ and $y = \eta(\boldsymbol{x}, t)$ are, respectively, the equations of the still level, of the impermeable horizontal bottom and of the free surface (impermeable or not). The velocity potential ϕ is defined by $\boldsymbol{u} = \nabla\phi$ and $v = \phi_y$, where ∇ is the horizontal gradient, $\boldsymbol{u} = (u_1, u_2)$ and v being the horizontal and vertical velocities, respectively. We denote with 'tildes' the quantities at the surface, e.g., $\tilde{\phi}(\boldsymbol{x}, t) = \phi(\boldsymbol{x}, \eta(\boldsymbol{x}, t), t)$.

At the free surface, the pressure p (per unit mass) involves a generating pressure $\tilde{p}_{\mathrm{G}}$ (i.e., a pneumatic wave maker) and a dissipative pressure $\tilde{p}_{\mathrm{D}}$ (i.e., a wave absorber); this notation being convenient. $\tilde{p}_{\mathrm{G}}$ and $\tilde{p}_{\mathrm{D}}$ are defined in Sections 3 and 4, respectively. In addition, we also allow a possible damping term $\tilde{v}_{\mathrm{D}}$ in the surface kinematic condition. This means that if $\tilde{v}_{\mathrm{D}} \neq 0$ the surface is not impermeable, i.e., the mass is not conserved. The role and definition of $\tilde{v}_{\mathrm{D}}$ are given in Section 4.3. Hence, the kinematic and dynamic conditions at the surface can then be conveniently written (without surface tension)

$$\eta_t - V = \tilde{v}_{\mathrm{D}}, \tag{1}$$

$$\tilde{\phi}_t + g\eta + \tfrac{1}{2}\tilde{\boldsymbol{u}} \cdot \nabla\tilde{\phi} - \tfrac{1}{2}\tilde{v}V = -\tilde{p}_{\mathrm{G}} - \tilde{p}_{\mathrm{D}}, \tag{2}$$

where g is the acceleration of gravity, $V = \phi_n\sqrt{1 + |\nabla\eta|^2}$ (ϕ_n being the outward normal derivative of ϕ at the surface) and

$$\tilde{\boldsymbol{u}} = \frac{\nabla\tilde{\phi} - V\nabla\eta + (\nabla\eta \times \nabla\tilde{\phi}) \times \nabla\eta}{1 + |\nabla\eta|^2}, \quad \tilde{v} = \frac{V + \nabla\eta \cdot \nabla\tilde{\phi}}{1 + |\nabla\eta|^2}. \tag{3}$$

The Laplace equation and the bottom impermeability are solved exactly by means of a Green function and the method of images (Clamond and Grue [5, Section 6], Grue [8, Section 6]), i.e.

$$\int GV' \,\mathrm{d}\boldsymbol{x}' = 2\pi\tilde{\phi} + \int \tilde{\phi}' \frac{\partial G}{\partial n}\sqrt{1 + |\nabla'\eta'|^2}\,\mathrm{d}\boldsymbol{x}' \tag{4}$$

with

$$G = \frac{1}{\sqrt{(\boldsymbol{x}' - \boldsymbol{x})^2 + (\eta' - \eta)^2}} + \frac{1}{\sqrt{(\boldsymbol{x}' - \boldsymbol{x})^2 + (\eta' + \eta + 2h)^2}}, \tag{5}$$

where $\tilde{\phi} = \tilde{\phi}(\boldsymbol{x}, t)$, $\tilde{\phi}' = \tilde{\phi}(\boldsymbol{x}', t)$, etc., and with the convenient brief notation

$$\int \bullet \,\mathrm{d}\boldsymbol{x}' \equiv \int_{-\infty}^{\infty}\int_{-\infty}^{\infty} \bullet \,\mathrm{d}x_1'\,\mathrm{d}x_2'. \tag{6}$$

The integral equation (4) is inverted by means of Fourier transform. Further, it is advantageous to integrate the systems (1) and (2) in Fourier space. We hence introduce the Fourier transform $\mathfrak{F}$ as

$$\hat{q}(\boldsymbol{k}, t) = \mathfrak{F}\{q\} = \int q(\boldsymbol{x}, t)\,\mathrm{e}^{-\mathrm{i}\boldsymbol{k}\cdot\boldsymbol{x}}\,\mathrm{d}\boldsymbol{x},$$

$$q(\boldsymbol{x}, t) = \mathfrak{F}^{-1}\{\hat{q}\} = \frac{1}{4\pi^2}\int \hat{q}(\boldsymbol{k}, t)\,\mathrm{e}^{\mathrm{i}\boldsymbol{k}\cdot\boldsymbol{x}}\,\mathrm{d}\boldsymbol{k},$$

for any quantity q and where $\boldsymbol{k} = (k_1, k_2)$ are the wavenumbers.

3. Pneumatic wave makers

To generate waves from rest, we use a pneumatic wave maker, i.e., we prescribe a pressure distribution at the surface via the function $\tilde{p}_{\mathrm{G}}$ in (2). Pneumatic wave makers are numerically more efficient than paddle

wave makers. The singularity at the intersection between the free surface and a partially submerged paddle wave maker is avoided by using the pneumatic wave generator, for example. We consider here three types of pneumatic generation: (i) a purely oscillating multichromatic long-crested (two-dimensional) wave generator; (ii) a purely oscillating multichromatic axisymmetric wave generator; (iii) a moving (at constant speed and localized in space) non-oscillating pressure distribution. The latter is used to model ship generated waves. The linear theory of such generation is described by Wehausen and Laitone [13, Section 21]. Of course, all these wave makers can be duplicated and combined in several configurations. Such a generalization is straightforward.

3.1. Purely oscillating pressure distributions

A multichromatic wave (with J components) of angular frequencies $\sigma_j > 0$—that are all different constants and not necessarily integer multiples of, say, σ_1—is generated from rest choosing a pressure distribution of the form

$$\tilde{p}_{\mathrm{G}} = \sum_{j=1}^{J} \sin(\sigma_j t + \varphi_j) P_j(\boldsymbol{x}) H(t), \tag{7}$$

where φ_j are constant phase shifts, P_j are functions localized in space and H is the Heaviside function ($H = 0$ for $t < 0$, $H = 1$ for $t > 0$).

We then define below two special types of wave maker: (i) a long crested wave generator (2D) and (ii) an axisymmetric wave generator. Of course, other special combinations of wave makers can also be defined, as well as other generic function than (7).

3.1.1. Two-dimensional wave maker

To generate two-dimensional waves that propagate along the x_1-direction, say, the functions P_j are chosen of the form

$$P_j = A_j \mathrm{e}^{-x_1^2/2\lambda_j^2} \Longleftrightarrow \widehat{P}_j = \sqrt{2\pi} A_j \lambda_j \mathrm{e}^{-k_1^2\lambda_j^2/2} \delta(k_2), \tag{8}$$

where A_j and λ_j are constants and δ is the Dirac function. This even function is chosen because it is localized, smooth, monotonic and rapidly decaying in both physical and Fourier space.

For the wave maker to be efficient, it must transmit as much energy as possible to the far field. This means that the parameters A_j and λ_j cannot be taken arbitrarily. Therefore, to generate waves with amplitudes a_j and wavenumbers κ_j (given by $\sigma_j = \sqrt{g\kappa_j \tanh \kappa_j h}$) in the far field, one must take (according to the linear theory without surface tension, see [13, Section 21])

$$\lambda_j = \frac{1}{\kappa_j}, \quad A_j = g a_j \sqrt{\frac{\mathrm{e}}{2\pi}} \left(1 + \frac{2\kappa_j h}{\sinh 2\kappa_j h}\right). \tag{9}$$

The parameters a_j and φ_j can be taken ad libitum. For instance, they can be tuned to model a JONSWAP spectrum.

This wave maker has been successfully implemented in two-dimensional wave simulations [4,5]. It works as well to generate long-crested wave in three-dimensional simulations.

3.1.2. Cylindric wave maker

To generate J axisymmetric waves centered at $\boldsymbol{x} = \boldsymbol{x}_j$ ($1 \leqslant j \leqslant J$), we take a pressure distribution as

$$P_j = A_j \mathrm{e}^{-r_j^2/4\lambda_j^2} \Longleftrightarrow \widehat{P}_j = 4\pi A_j \lambda_j^2 \mathrm{e}^{-k^2\lambda_j^2} \mathrm{e}^{-\mathrm{i}\boldsymbol{k}\cdot\boldsymbol{x}_j} \tag{10}$$

with $r_j = |\boldsymbol{x} - \boldsymbol{x}_j|$, $k = |\boldsymbol{k}|$ and where A_j and λ_j are constants. To transmit as much energy as possible to the far field, given by the linear theory

$$\eta(\boldsymbol{x},t) \sim \sum_{j=1}^{J} a_j(\kappa_j r_j)^{-1/2} \cos\left(\kappa_j r_j - \sigma_j t - \varphi_j - \frac{1}{4}\pi\right) \text{ as } r_j \to \infty, \tag{11}$$

where $\sigma_j = \sqrt{g\kappa_j \tanh \kappa_j h}$, the parameters must be taken as (see [13, Section 21])

$$\lambda_j = \frac{1}{\kappa_j}, \quad A_j = \frac{\mathrm{e} g a_j}{\sqrt{8\pi}}\left(1 + \frac{2\kappa_j h}{\sinh 2\kappa_j h}\right). \tag{12}$$

The wave 'amplitudes' a_j, the 'wavenumbers' κ_j, the phase shifts φ_j and the positions of the wave makers $\boldsymbol{x}_j$ are free parameters.

3.2. Advancing pressure

To apply instantaneously from rest a pressure distribution that propagates at a constant speed v in the x_1-direction, we take a pressure distribution of the form

$$\tilde{p}_{\mathrm{G}} = P(x_1 - vtH(t), x_2) - \langle P_0(x_1,x_2)\rangle \Longleftrightarrow \hat{p}_{\mathrm{G}} = \widehat{P}_0(\boldsymbol{k})\,\mathrm{e}^{-\mathrm{i}k_1 vtH(t)} - \langle P_0\rangle\delta(\boldsymbol{k}), \tag{13}$$

where P is a function localized in space, $P_0 = P(t = 0)$ and $\langle\bullet\rangle$ is the spacial average operator. The pressure distribution (13) is chosen in such a form because for $t < 0$, the pressure distribution in the fluid is hydrostatic, $\tilde{\phi} = 0$, $\eta = -\tilde{p}_{\mathrm{G}}/g$ and $\langle\eta\rangle = 0$.

For similar reasons as above, we consider the convenient well-behaved function

$$P_0 = A\,\mathrm{e}^{-\frac{x_1^2}{\lambda_1^2} - \frac{x_2^2}{\lambda_2^2}} \Longleftrightarrow \widehat{P}_0 = \pi\lambda_1\lambda_2 A\,\mathrm{e}^{-(k_1^2\lambda_1^2 + k_2^2\lambda_2^2)/4}, \tag{14}$$

where A and λ_i are constants (not necessarily positive). If $\lambda_1 \neq \lambda_2$, the pressure distribution has an ellipse-like shape. This means that the parameters can be chosen to model the wave generation by an elongated body (ship), for example.

We note that, with a temporal variation of the velocity as $v(t)H(t)$, the acceleration is infinite at $t = 0$. This is not a problem for the numerical stability of the model (see below), that is an advantage of pneumatic generations.

3.3. Analytic linear solution

As mentioned in Part I, our numerical model involves an exact analytic integration of the linear part of the equations, including the contribution due to the generating pressure (but not the damping terms). For various pressure distributions, linear solutions of the wave field can be found in many references (e.g. [13]). These formulae are generally written in analytic forms involving apparent singularities, not suitable for numerical calculations. To overcome this difficulty, using some trigonometric identities, we have carefully written the solution without apparent singularities. The solution is as follow.

At a time t_0 the surface elevation is $\eta_0(\boldsymbol{x})$ and the velocity potential is $\tilde{\phi}_0(\boldsymbol{x})$. Hence, at any time $t > t_0$ the linearized solution of the initial value problem—without the damping terms $\tilde{v}_{\mathrm{D}}$ and $\tilde{p}_{\mathrm{D}}$, in Fourier space and with the notations defined in Section 2—is (see Part I, Section 3.3)

$$\hat{\eta}(\boldsymbol{k},t) = \hat{\eta}_0 \cos\omega(t - t_0) + (\omega/g)\hat{\phi}_0 \sin\omega(t - t_0) + \widehat{R}_\eta(\boldsymbol{k},t), \tag{15}$$

$$\hat{\phi}(\boldsymbol{k},t) = \hat{\phi}_0 \cos\omega(t - t_0) - (g/\omega)\hat{\eta}_0 \sin\omega(t - t_0) + \widehat{R}_\phi(\boldsymbol{k},t), \tag{16}$$

where $\omega = \sqrt{gk\tanh kh}$ and

$$\widehat{R}_\eta = -\frac{\omega}{g}\int_{t_0}^{t} \hat{p}'_{\mathrm{G}} \sin\omega(t-t')\,\mathrm{d}t', \quad \widehat{R}_\phi = -\int_{t_0}^{t} \hat{p}'_{\mathrm{G}} \cos\omega(t-t')\,\mathrm{d}t' \tag{17}$$

with $\hat{p}'_{\mathrm{G}} = \hat{p}_{\mathrm{G}}(\boldsymbol{k}, t')$.

For a purely oscillating wave maker of the general form (7), after some algebra we obtain

$$\widehat{R}_\eta = \sum_{j=1}^{J} \widehat{P}_j \frac{\omega/g}{\omega+\sigma_j}\left\{\sin(\sigma_j t_0+\varphi_j)\cos\omega T^- - \sin(\sigma_j t+\varphi_j) + \sigma_j T^- \operatorname{sinc}\frac{(\omega-\sigma_j)T^-}{2}\cos\frac{\omega T^- + \sigma_j T^+ + 2\varphi_j}{2}\right\}, \tag{18}$$

$$\widehat{R}_\phi = -\sum_{j=1}^{J} \widehat{P}_j \frac{1}{\omega+\sigma_j}\left\{\sin(\sigma_j t_0+\varphi_j)\sin\omega T^- + \sigma_j T^- \operatorname{sinc}\frac{(\omega-\sigma_j)T^-}{2}\sin\frac{\omega T^- + \sigma_j T^+ + 2\varphi_j}{2}\right\}, \tag{19}$$

where $T^\pm = t \pm t_0$, $\operatorname{sinc} x = \sin x/x$ and $\operatorname{sinc} 0 = 1$. Since $\omega \geqslant 0$ and $\sigma_j > 0$, $\omega + \sigma_j$ is never zero and, therefore, these relations are written in a form without apparent singularities, which is an important feature in numerical computations.

For an advancing pressure distribution of the form (13), we have

$$\widehat{R}_\eta = \frac{\mathrm{i}\omega\widehat{P}_0\,\mathrm{e}^{-\mathrm{i}\sigma t_0}}{g(\omega+\sigma)}\left\{\sin\omega T - \omega T\operatorname{sinc}\frac{(\omega-\sigma)T}{2}\,\mathrm{e}^{-\frac{\mathrm{i}}{2}(\omega+\sigma)T}\right\}, \tag{20}$$

$$\widehat{R}_\phi = -\frac{\widehat{P}_0\,\mathrm{e}^{-\mathrm{i}\sigma t_0}}{\omega+\sigma}\left\{\sin\omega T + \sigma T\operatorname{sinc}\frac{(\omega-\sigma)T}{2}\,\mathrm{e}^{-\frac{\mathrm{i}}{2}(\omega+\sigma)T}\right\} + \langle P_0\rangle T\delta(\boldsymbol{k}), \tag{21}$$

where $\sigma = k_1\upsilon$ and $T = t - t_0$. Here, $\omega \geqslant 0$ but σ is real, so that $\omega + \sigma$ can be zero. However, because we are dealing with Fourier transforms of real functions, it is sufficient to define $\widehat{R}$ for $\sigma > 0$ (i.e., for $k_1 > 0$ if $\upsilon > 0$) and then to obtain $\widehat{R}$ for $\sigma < 0$ taking the complex conjugate.

4. Absorbing dynamic boundary condition

For non-periodic problems, one must provide conditions at the open boundaries. To absorb outgoing waves and avoid incoming ones, we present here an efficient modified version of the so-called *sponge layer* technique [9,12]. We have implemented a new modified sponge layer via a damping pressure of the form

$$\tilde{p}_{\mathrm{D}} = \nabla^{-1}\cdot\left(\gamma\nabla\tilde{\phi}\right) - B(t), \tag{22}$$

where γ is a non-zero function of the space coordinate in the regions where damping is required and zero elsewhere. ∇ is the horizontal gradient operator and B is a Bernoulli constant. The inverse operator is defined by $\nabla^{-1} = \Delta^{-1}\nabla$, Δ being the horizontal Laplacian. In practice, ∇^{-1} is easily computed via Fourier transform

$$\nabla^{-1}\cdot\left(\gamma\nabla\tilde{\phi}\right) = \mathfrak{F}^{-1}\left\{\frac{\mathrm{i}\boldsymbol{k}}{-k^2}\cdot\mathfrak{F}\left\{\gamma\nabla\tilde{\phi}\right\}\right\}. \tag{23}$$

Introducing (22) into the dynamic boundary condition (2), we obtain

$$\tilde{\phi}_t + \nabla^{-1}\cdot\left(\gamma\nabla\tilde{\phi}\right) + T = B(t), \tag{24}$$

where $T = g\eta + \frac{1}{2}\tilde{\boldsymbol{u}} \cdot \nabla\tilde{\phi} - \frac{1}{2}\tilde{v}V + \tilde{p}_{\mathrm{G}}$. Taking the horizontal gradient of (24) one obtains

$$\boldsymbol{U}_t + \gamma \boldsymbol{U} + \nabla T = 0, \tag{25}$$

where $\boldsymbol{U} = \nabla\tilde{\phi} = \boldsymbol{V}_{\mathrm{T}}\sqrt{1 + |\nabla\eta|^2}$ and $\boldsymbol{V}_{\mathrm{T}}$ denotes the fluid velocity tangential to the free surface. Thus, the method rather damps the (physical) tangential fluid velocity at the surface than the velocity potential.

With an absorber of the form (22), all frequencies are damped with the same intensity. This can be easily seen considering the Fourier transform of $\tilde{p}_{\mathrm{D}}$ with a constant γ. Further, the important Bernoulli constant (see below) vanishes in our implementation since we solve numerically Eq. (24) in Fourier space multiplied by $k\omega/g$ (see Part I), but other methods of resolution may require an explicit treatment of the Bernoulli constant.

Note that the relation (23) is not defined for $\boldsymbol{k} = \boldsymbol{0}$. This value plays the role of an integration constant and must be imposed in accordance to a mean level and the frame of reference. Note also that for numerical methods other than pseudo-spectral, e.g., finite differences, the computation of ∇^{-1} requires the calculus of Δ^{-1} that can be obtained solving a linear system of equations (i.e., inversion of a matrix).

We have found that absorbing beaches of the form (22) are highly effective (see Section 5). We shall now justify this choice. This justification requires first to understand why classical sponge layers are not very effective. Then, the new absorber will appear naturally.

4.1. Discussions and justifications

4.1.1. Bernoulli equation with dissipation

Fluid flows in porous media can be modelled with the well-known Darcy law $\vec{\mathrm{v}} = -\gamma^{-1}\operatorname{grad}\mathscr{H}$, where γ is the permeability and $\mathscr{H}$ is the hydraulic head. For homogeneous media (constant γ), this law implies a potential flow, and Darcy's equation can thus be integrated into a Bernoulli equation with a dissipative term

$$\phi_t + \gamma\phi + \tfrac{1}{2}(\operatorname{grad}\phi)^2 + gy + p = B(t), \tag{26}$$

where B is a Bernoulli 'constant' and p is the pressure (per unit of mass). Note that in some applications of fluid mechanics, γ is sometimes called the Rayleigh (outer) viscosity.

By analogy with flows in porous media, the *sponge layer absorption* of surface waves consists in introducing, into Eq. (2), a damping pressure of the type

$$\tilde{p}_{\mathrm{D}} = \gamma\tilde{\phi} - B \tag{27}$$

with $\gamma(\boldsymbol{x}) \neq 0$ where damping is required. The surface dynamic condition (2) can then be conveniently rewritten

$$\tilde{\phi}_t + \gamma\tilde{\phi} + T = B, \tag{28}$$

where the function T is given below Eq. (24). The Bernoulli equation with dissipation (28) is thus a generalization of (26) for a variable permeability, and is formulated with the purpose to absorb waves. Note that such a generalization cannot be derived from the Darcy law—because Darcy's law implies a rotational flow if γ is not constant—and is thus artificial.

Although a variable γ is artificial and not completely physical, this equation must respect some physical principles. Otherwise, undesirable spurious effects appear and the efficiency of the absorbing beach decreases.

4.1.2. Validity of the Bernoulli equation with dissipation

To absorb waves, the physical quantities (e.g., velocity, energy) must be damped. ϕ itself is not totally physical because it is defined via a mathematical transformation: an integration. Adding any constant to ϕ does not

change the velocity field (see below). With a Bernoulli equation with constant dissipation, $\tilde{\phi}$ is damped toward B/γ. Thus, arises the question: *Why damping $\tilde{\phi}$ toward B/γ and not toward any other quantity?*

If γ is constant, it is easy via gauge transformations $\tilde{\phi} \mapsto \tilde{\phi}^{\bigstar}$ and $B \mapsto B^{\bigstar}$, to verify that any choice can be obtained from any other one. It is therefore equivalent to damp $\tilde{\phi}$ toward B/γ or toward any other quantity.

This is not true if γ varies, however, because the gauge transformations do not preserve the velocity field, see Section 4.2.2. Therefore, damping $\tilde{\phi}$ is physically meaningless when γ is not a constant.

The Bernoulli equation with dissipation (26) is a valid model for fluid flows in homogeneous porous media only. This is not a physically consistent one for heterogeneous media. Therefore, such an equation cannot be used for wave damping, and a 'more physical' equation must be preferred.

4.1.3. Justification of the modified Bernoulli equation with dissipation

The modified equation (24) can be justified with some mathematical and physical arguments. To do so, it suffices to take the horizontal gradient of (28), giving

$$\boldsymbol{U}_t + \gamma \boldsymbol{U} + (\nabla\gamma)\nabla^{-1} \cdot \boldsymbol{U} + \nabla T = 0. \tag{29}$$

In the left-hand side of (29), the term $[\partial_t + \gamma]$ acts as a dissipative (parabolic) operator on $\boldsymbol{U}$, while the (hyperbolic) operator $[\partial_t + (\nabla\gamma)\nabla^{-1}\cdot]$ allows the propagation of waves (i.e., $\boldsymbol{U}_t + (\nabla\gamma)\nabla^{-1} \cdot \boldsymbol{U} = 0$ is a kind of wave equation). Therefore, if $|\nabla\gamma|$ is large, the left-hand side of (29) mainly acts as a wave propagator, which is an undesirable property for the absorption of waves.

Purely dissipative linear operators involve $\boldsymbol{U}$'s spatial derivatives (or antiderivatives) of even orders only in order to get a parabolic operator. A dissipative equation is then obtained cancelling the term $(\nabla\gamma)\nabla^{-1} \cdot \boldsymbol{U}$ in the relation (29) and integrating the resulting equation. One thus obtains a modified Bernoulli equation with dissipation, namely Eq. (24).

4.2. Remarks

4.2.1. Low-pass filters

Low-pass filters have been proposed [11] via a viscous-like damping, the damping pressure taking the form

$$\tilde{p}_{\mathrm{D}} = -\nu\Delta\tilde{\phi} - B \tag{30}$$

with $\nu(\boldsymbol{x}) \neq \boldsymbol{0}$ where viscous damping is required. For a non-constant coefficient ν, and according to the discussion above, a more physical viscous-like damper would be given by

$$\tilde{p}_{\mathrm{D}} = -\nabla^{-1} \cdot \left\{ \nu\nabla\Delta\tilde{\phi} \right\} - B. \tag{31}$$

Viscous dampers involve high-order derivatives that induce stiffness into the numerical resolution, however. The computational time is then increased significantly. Such a damper should therefore be used for well defined purposes and not as general dampers.

Damping proportional to the normal velocity at the surface have also been employed. The purpose has been to avoid important reflections caused by the classical sponge damper when γ is large. In our notation such a damper reads

$$\tilde{p}_{\mathrm{D}} = \gamma\phi_n - B. \tag{32}$$

This damper does not reflect waves but it is not very effective in damping outgoing waves. It is therefore not suitable for periodic computational boxes since it causes large wave transmission. Due to the involvement of ϕ's derivative, this damper induces numerical stiffness and—for the same damping effect as with the new damper (22)—the computational time can be increased by several orders of magnitude. This is therefore not a efficient damper for practical purposes.

4.2.2. Bernoulli constant and gauge condition

A velocity potential—being defined via its gradient—is not unique. Its uniqueness must then be enforced adding an extra condition: a so-called *gauge condition* in theoretical physics. When $\gamma = 0$, a usual gauge is obtained taking $B = 0$ since the transformation

$$\tilde{\phi} = \tilde{\phi}^{\star} + \int_{t_0}^{t} B(t')\,\mathrm{d}t', \tag{33}$$

lets the Bernoulli equation unchanged except that B vanishes. Similarly, when $\gamma \neq 0$ is constant, the transformation

$$\tilde{\phi} = \tilde{\phi}^{\star} + \int_{t_0}^{t} B(t')\,\mathrm{e}^{\gamma(t'-t)}\,\mathrm{d}t', \tag{34}$$

applied to (28), yields a Bernoulli equation with dissipation and $B = 0$. Thus, with an appropriate definition of $\tilde{\phi}$, B can be zero without loss of generality. Conversely, the choice $B = 0$ enforces the uniqueness of ϕ and preserves the velocity field (i.e., $\nabla\tilde{\phi} = \nabla\tilde{\phi}^{\star}$).

On the other hand, if γ is not a constant, $B = 0$ is no longer a valid gauge because the transformation (34) yields

$$\nabla\tilde{\phi} = \nabla\tilde{\phi}^{\star} + (\nabla\gamma)\int_{t_0}^{t} (t'-t)B(t')\,\mathrm{e}^{\gamma(t'-t)}\,\mathrm{d}t', \tag{35}$$

so that $\nabla\tilde{\phi} \neq \nabla\tilde{\phi}^{\star}$ if $\nabla\gamma \neq \mathbf{0}$. This means that the equation is modified with extra terms involving $\nabla\gamma$. No simple transformation leads to an equation with $B = 0$. Indeed, $\tilde{\phi} = \tilde{\phi}^{\star} + f(t)$ is the most general transformation satisfying $\nabla\tilde{\phi} = \nabla\tilde{\phi}^{\star}$. Obviously, no choice of f leads to an equation for $\tilde{\phi}^{\star}$ with $B = 0$ if γ is not constant.

In conclusion, when a Bernoulli equation is used with a variable γ together with $B = 0$, $\nabla\tilde{\phi}$ is *not* the velocity field in the neighborhood of $\nabla\gamma \neq \mathbf{0}$. The equation then looses its consistency and unphysical phenomena (e.g., wave emissions) appear, a problem which has long been observed.

4.3. Mass absorption

With dynamic absorbers, as the ones presented above, the velocity (and thus the kinetic energy) is damped, but the mass is conserved. In some situations, however, the mass should not be conserved. An example is a solitary wave leaving the computational domain. In this case, if only the velocity is damped, the finite amount of mass carried by the wave is spread in all the domain. Thus, in order to avoid this problem, the mass must be damped too.

To damp the mass, by analogy with the damping in the Bernoulli equation with dissipation, we introduce in the kinematic equation a damping term of the form

$$\tilde{v}_{\mathrm{D}} = -\Gamma\eta, \tag{36}$$

where $\Gamma \geqslant 0$ is not zero in the regions where damping is required. We note that the Γ in (36) is not necessarily identical to the parameter γ involved in $\tilde{p}_{\mathrm{D}}$. Such a damper for the surface elevation has been considered by several authors (e.g. [2,3]).

5. Numerical tests

The generation of two-dimensional waves has already been investigated in the two-dimensional version of the model [4,5]. Using the present three-dimensional model, we have verified that long crested waves are as well generated. We thus focus here on the generation of axisymmetric waves and "ship-waves".

5.1. Absorption of an axisymmetric wave by a circular damper

The variations of the damper must be smooth enough to avoid numerical instabilities. For instance, we consider a circular damper built upon a Gaussian function as

$$\gamma = \gamma_0 \, \mathrm{e}^{-\frac{(x-x_0)^2}{\lambda^2}}, \tag{37}$$

where $\gamma_0 = 1$, λ and x_0 are constants, and $x = |\boldsymbol{x}|$. The squared computational domain includes the outer and inner regions of the damper (Fig. 1).

At the centrum of the domain, we generate from rest a monochromatic axisymmetric wave with $\kappa h = 0.7$ and $a\kappa = 0.15$, the parameters a and κ being the far-field amplitude and wavenumber, respectively, appearing in the relation (11), with one wave component only. The computational domain is $8\pi \times 8\pi$ periodic, discretized over 128×128 nodes and the fully non-linear evolution is computed up to eighteen periods. No mass damping is used ($\Gamma = 0$).

After eighteen periods and without damper, the wave has travelled several times across the domain and the wave field is rather complex (Fig. 2(a)).

The same simulation with the present damper—Eq. (22) with $\tilde{p}_{\mathrm{D}} = \nabla^{-1} \cdot (\gamma \nabla \tilde{\phi}) - B(t)$—shows that all the outgoing waves have been absorbed. This can be seen from the fact that the surface exterior to the damping region is flat (Fig. 2(b)).

Conversely, with the dynamic damper $\gamma \phi_n$, a substantial part of the outgoing waves is not absorbed (Fig. 2(c)). Moreover, the computation of this damper is more than 20 times slower than with Eq. (22), due to the stiffness induced by ϕ_n. A stronger damping can be obtained increasing the magnitude of γ in the term $\gamma \phi_n$. This also increases the numerical stiffness and the computation becomes disastrously expensive, however. We conclude that this damper is not competitive for practical simulations.

We note that the classical sponge damper is about as effective as the previous one (Fig. 2(d)). Actually, it is not as bad as one may have thought, if the Bernoulli constant is treated properly. It is not as efficient as the damper (22), however.

This test clearly demonstrates the superiority of the new damper.

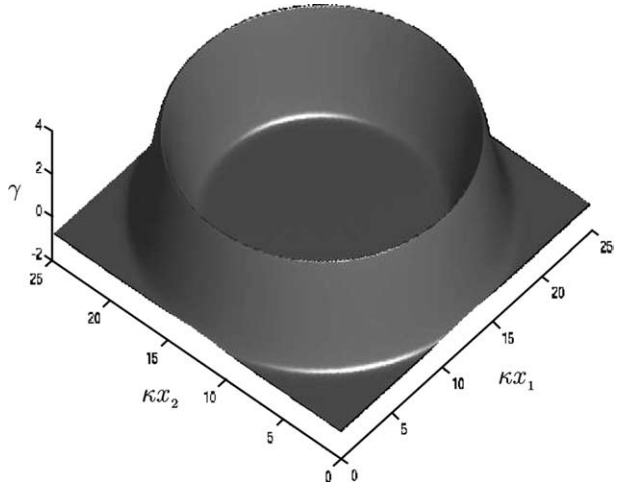

Fig. 1. Example of a circular damper.

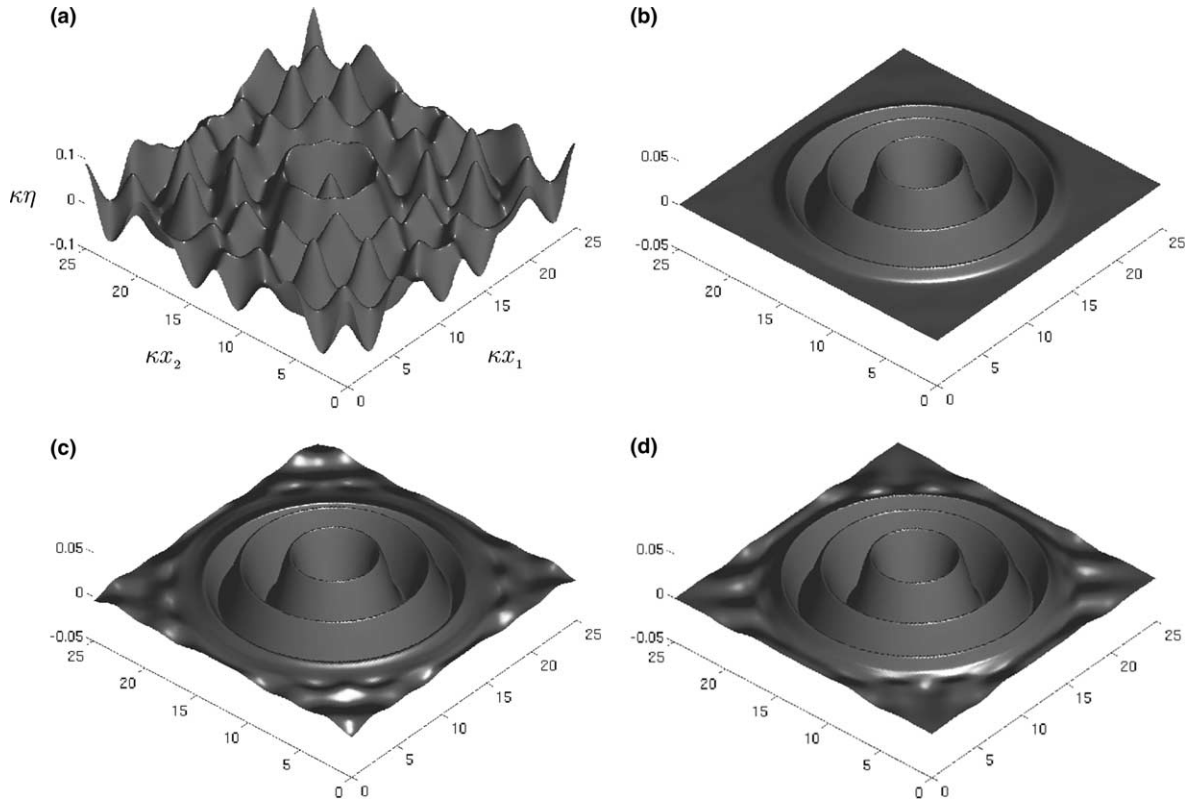

Fig. 2. Absorption of an axisymmetric wave by a circular damper: free surface after 18 periods. (a) No damper, (b) damper $\nabla^{-1}\cdot(\gamma\nabla\phi)$, (c) damper $\gamma\phi_n$, (d) damper $\gamma\phi$.

5.2. Complex geometries

With the present method it is very easy to define the damping functions γ and Γ that are not zero in various parts of the computational domain. Defining piece-wise the damping functions—with the help of Gaussian and tanh-functions, for example—one can model complex beach geometries.

An example of such non-trivial damping region is given in Fig. 3(a). For this example, there is no mass absorption ($\Gamma = 0$) and the depth is infinite. As previously, a monochromatic axisymmetric wave is generated from rest. The wave progressively fills the domain up to the time when a steady regime is obtained (Fig. 3(b) and (c)). Neither significant reflection nor transmission are observed. Indeed, if reflection or transmission were taking place, the energy could not remain constant.

This test demonstrates that the new damper has good absorbing properties, no matter what are the geometry and wave field.

5.3. Damping of a steep solitary wave

The efficiency of the present damper—Eq. (22)—together with the mass damping (36) is demonstrated computing the absorption of a large solitary wave with $a/h = 0.6$, a being the wave amplitude and h the (constant) water depth. This is a severe test since this wave is very energetic.

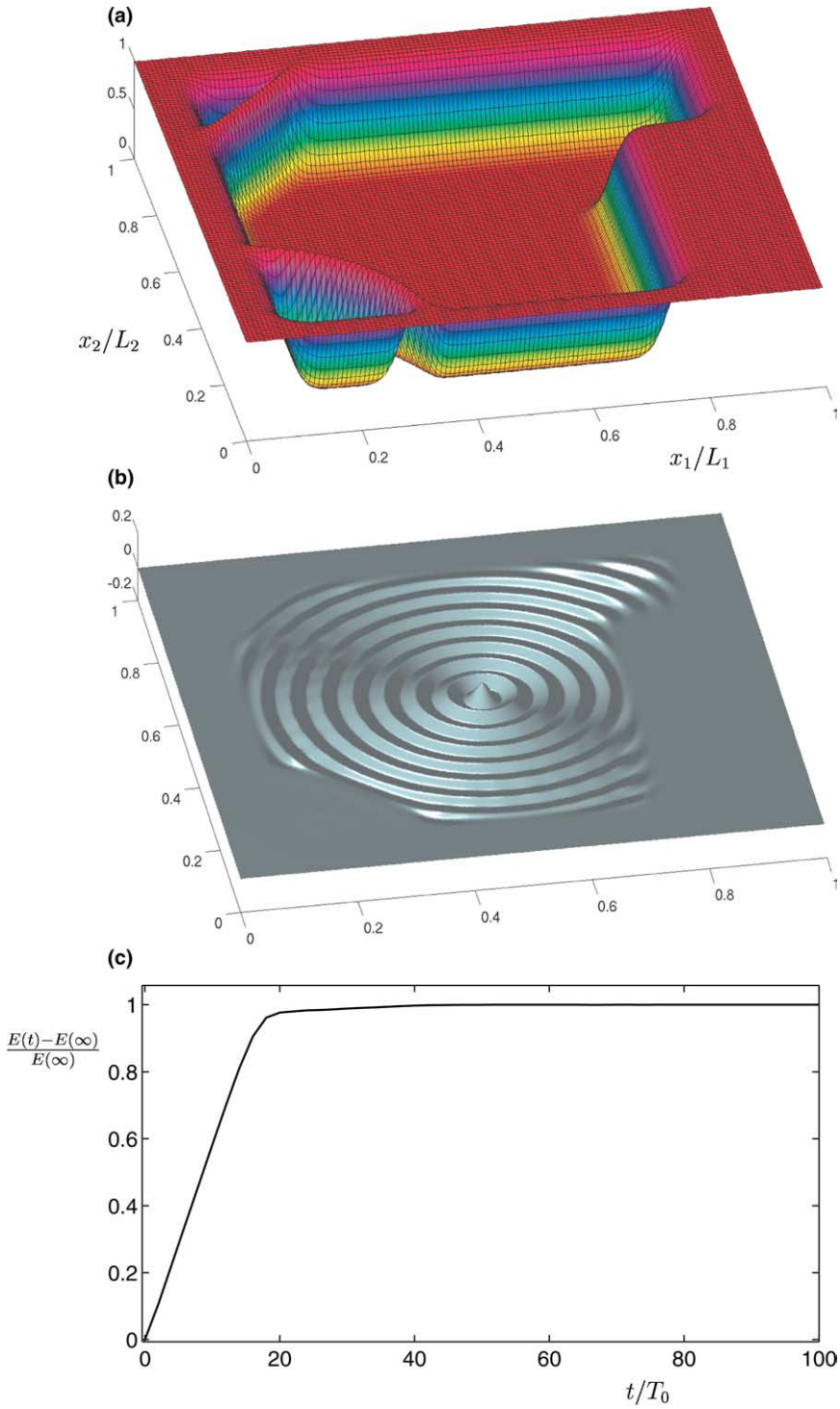

Fig. 3. Absorption of an axisymmetric wave by a complex damper. (a) Damper shape, (b) surface at $t = 100T_0$, (c) total energy variations.

The numerical basin is discretized with 4096×32 nodes in the x_1- and x_2-directions (the soliton propagates in the x_1-direction), with $\Delta x_1/h = 0.2$ and $\Delta x_2/h = 0.3$. Note that only a portion of the computational domain is plotted in Figs. 4 and 5. We employ absorbers defined by

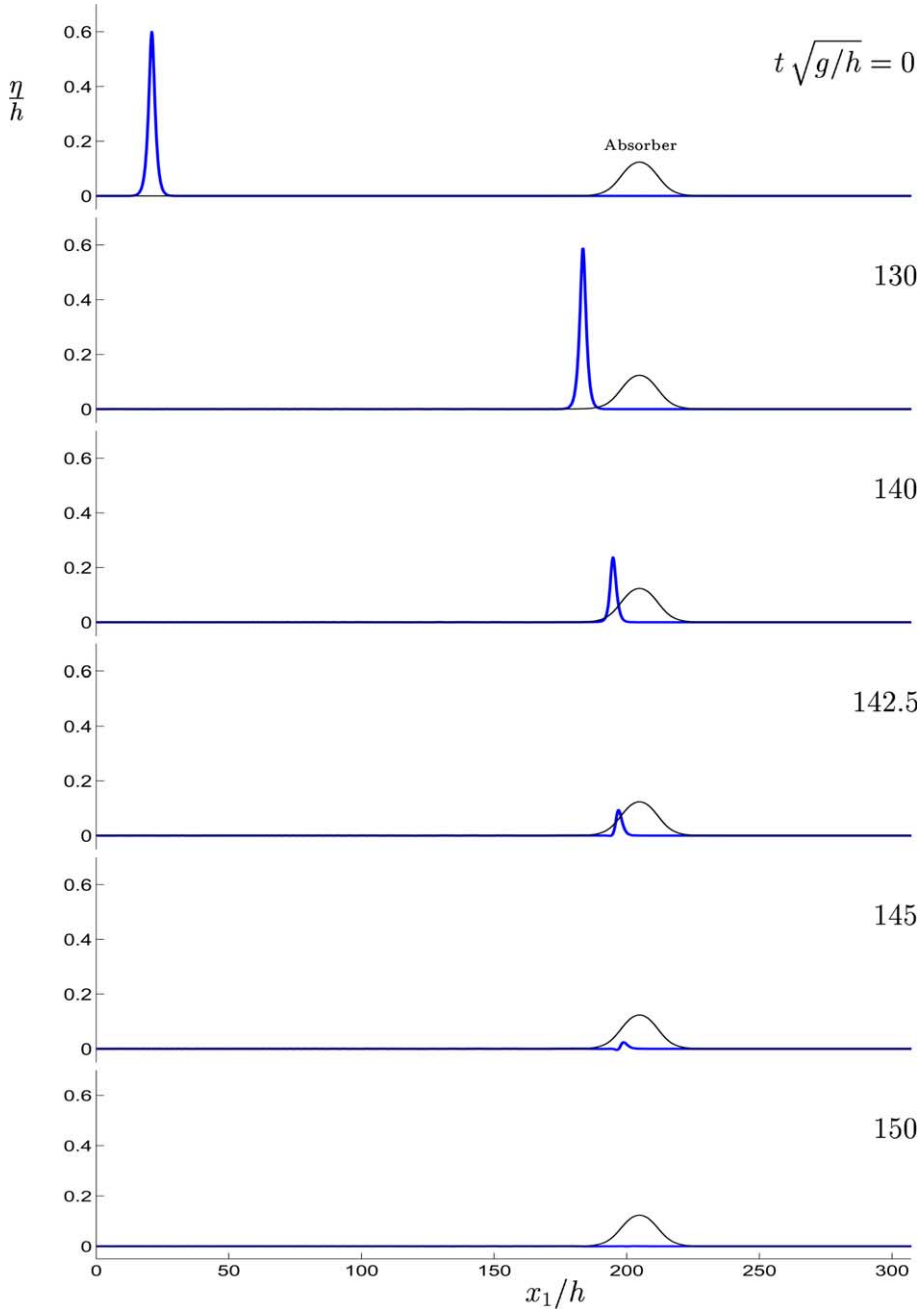

Fig. 4. Absorption of a soliton by the $\nabla^{-1} \cdot (\gamma \nabla \phi)$ and $\Gamma \eta$ dampers. (—) surface at $t = \{0; 130; 140; 142.5; 145; 150\}\sqrt{h/g}$, (——) profile of the damper.

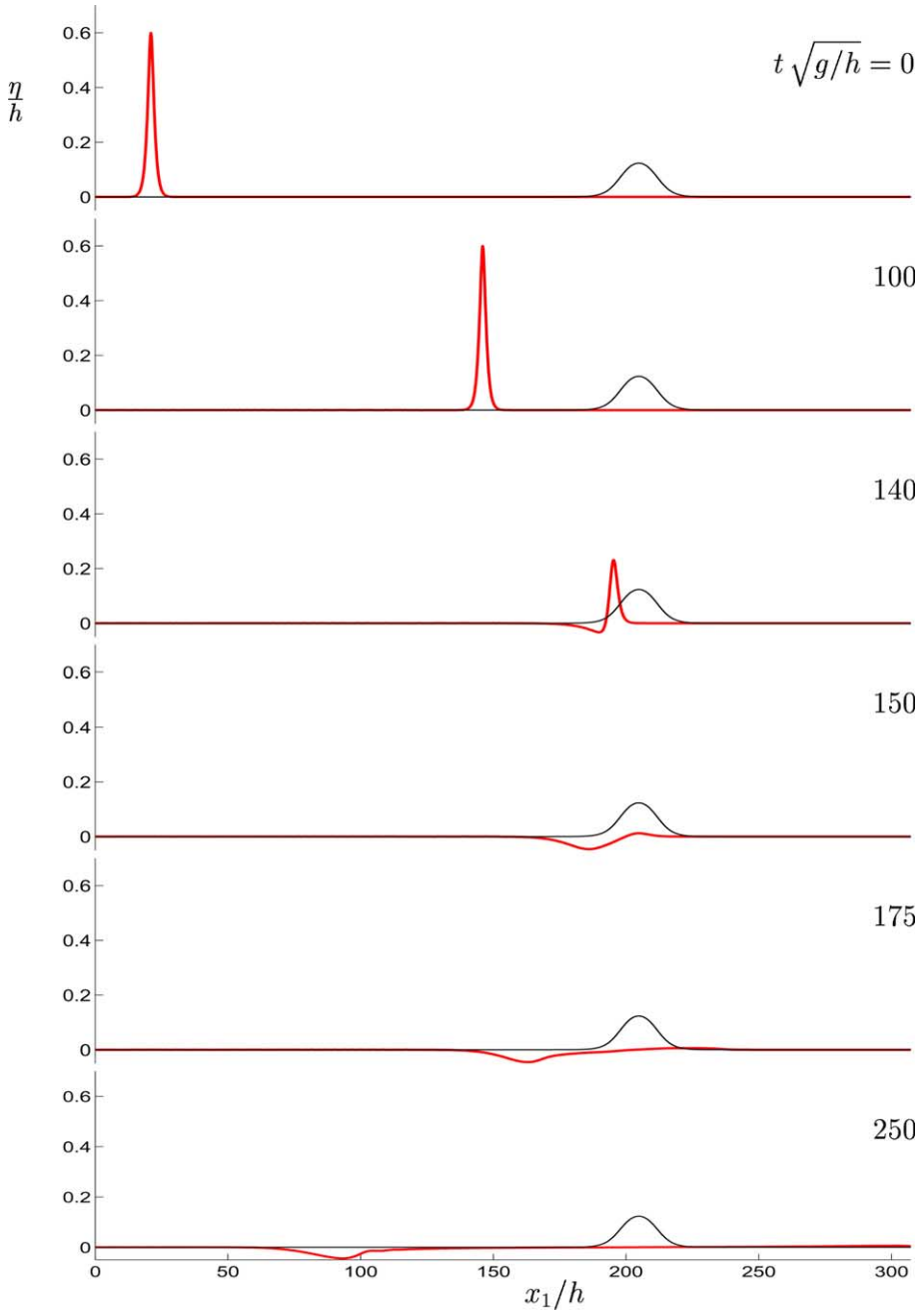

Fig. 5. Absorption of a soliton by the $\gamma\phi_n$ and $\Gamma\eta$ dampers. (—) surface at $t = \{0; 100; 140; 150; 175; 250\}\sqrt{h/g}$, (——) profile of the damper.

$$\gamma = \frac{\gamma_0}{2}\left[\tanh\left(\frac{x_1 - x_0 + \Lambda}{\alpha}\right) - \tanh\left(\frac{x_1 - x_0 - \Lambda}{\alpha}\right)\right], \quad \Gamma = \kappa\gamma, \tag{38}$$

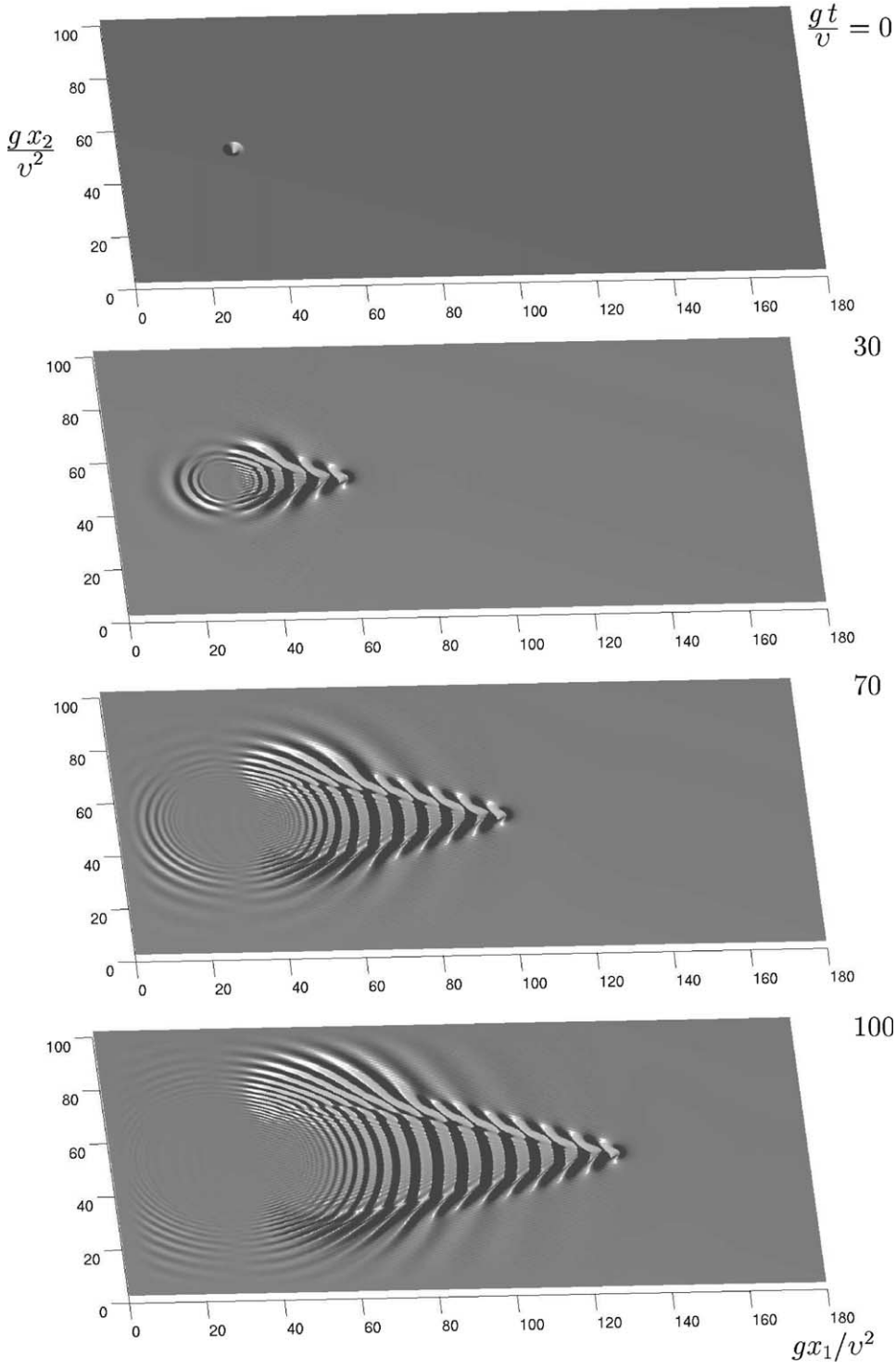

Fig. 6. Waves generated by a moving pressure. Free surface at $gt/v = \{0; 30; 70; 100\}$.

where the free parameters γ_0, κ, Λ, α and x_0 are tuned to obtain maximum damping according to the physics involved and the numerical parameters chosen. For the examples presented here, we have taken: $x_0/h = 205$, $\gamma_0 = 1$, $\Lambda/h = 6.83$, $\alpha/h = 5.85$, $\kappa = 1.07$.

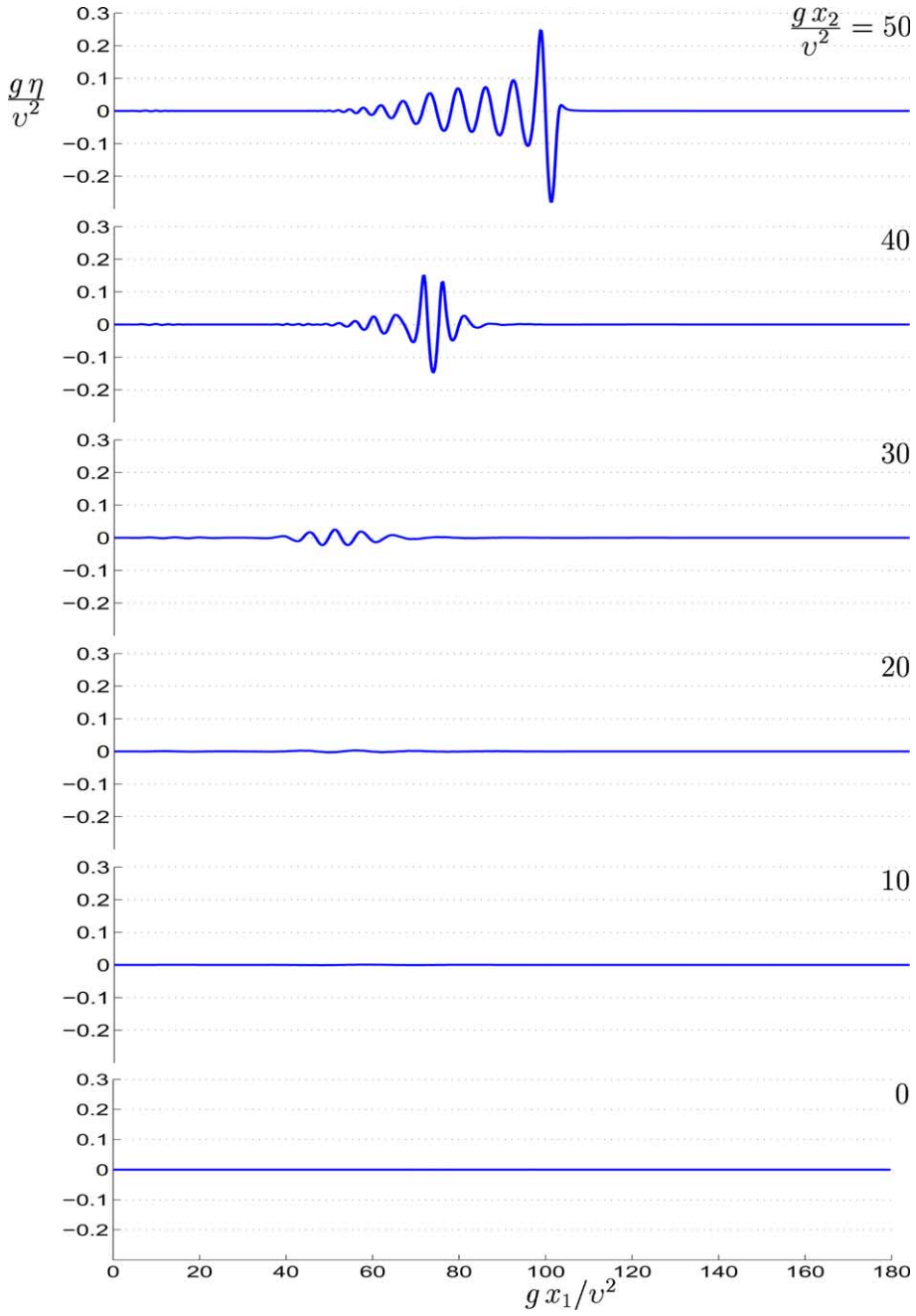

Fig. 7. Longitudinal slices of Fig. 6 at $gt/v = 70$.

With the damper in (22) (together with the mass absorber and with the parameters defined above) the solitary wave is effectively damped without significant reflection or transmission (Fig. 4). On the other hand, the damper of the form $\gamma\phi_n$ (together with the mass absorber and with the same parameters as in Fig. 4) does not absorb completely the wave. An important reflected wave is formed as well as a small trans-

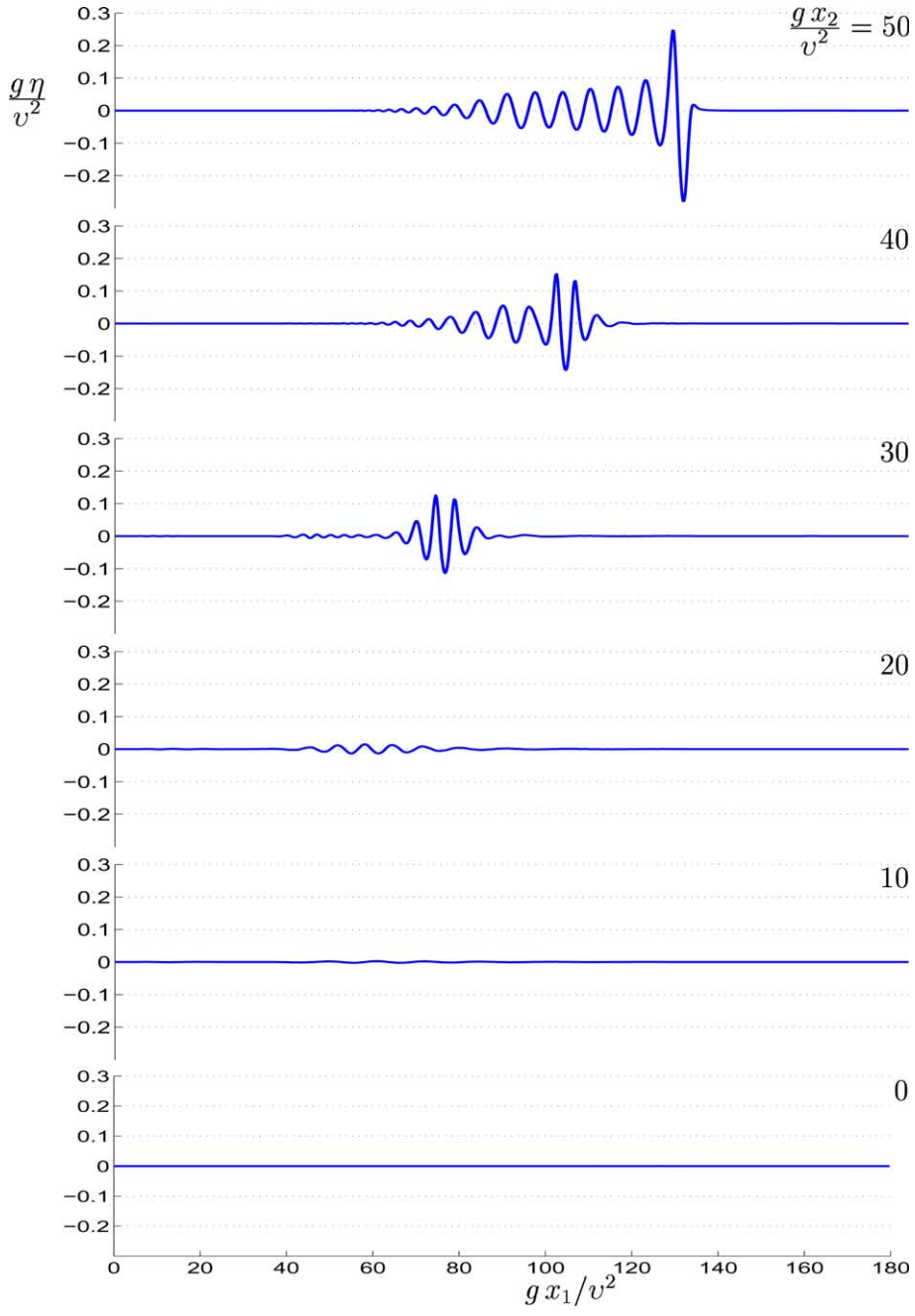

Fig. 8. Longitudinal slices of Fig. 6 at $gt/v = 100$.

mitted one (Fig. 5). This damper is obviously less efficient than the one in (22). Moreover, the computational time is more than doubled due to the numerical stiffness induced by the normal derivative of ϕ. Note that a damper $\gamma\phi_n$ alone, i.e., without mass absorption ($\Gamma = 0$) does not reflect waves, but it transmits a large amount of energy, and is not suitable for periodic domains.

5.4. Advancing pressure

We consider now the sudden motion of a pressure distribution as defined in Section 3.2, with $\lambda_1 = \lambda_2 = 1$, $\upsilon = 1$ and $A/g\lambda_1 = 0.15$. The computational domain involves 768×384 nodes and the depth is infinite. To absorb the outgoing ripples, the computational domain is bordered by a rectangular sponge absorber.

As shown in Fig. 6, the sudden start of the pressure induces waves but no numerical instabilities. As the pressure distribution progresses, the Kelvin ship-wave pattern is formed. At $gt/\upsilon = 100$, the maximum slope is $\max|\nabla\eta| = 0.41$, meaning that strong non-linear effects take place. The steep pressure generated waves are further illustrated in Figs. 7 and 8 showing slices of the surface elevation, for a selection of lateral coordinate, i.e., $gx_2/\upsilon^2 = 0$ (the outer boundary), 10, 20, 30, 40, 50 (mid-tank position), longitudinal coordinate in the range $0 < gx_1/\upsilon^2 < 180$, at times $gt/\upsilon = 70$ (Fig. 7) and $gt/\upsilon = 100$ (Fig. 8). It can be seen in these figures that at the position $gx_2/\upsilon^2 = 0$ corresponding to one side of the sponge layer, no waves are observed. At $gx_2/\upsilon^2 = 50$, the mid-tank position, the surface elevation is locally very steep.

This simulation demonstrates the effectiveness of the moving pressure distribution for modelling the formation of ship-waves in the intermediate and far field, as well as the efficiency of the non-singular analytic solution (20) and the robustness of the numerical model in general.

6. Conclusion

In this paper, we have described how to generate fully non-linear waves in a numerical wave tank, and how to efficiently damp the generated waves at an arbitrary boundary of the computational domain. The wave generation and damping procedures complement an efficient numerical scheme for fully non-linear surface wave simulations. The water is either of finite or infinite depth. The rapid potential formulation in periodic computational domains (without wave generation or damping) is described in full in the accompanying Part I of the paper [7].

Wave fields are generated by means of pneumatic wave makers. Starting out with results from linear theory, the wave makers are optimized for efficient fully non-linear generation in three dimensions. An important point of the procedure is an analytical integration of the linear part of the applied free surface pressure. This linear part is obtained in explicit form, valid for all times of the simulation. The linear expressions are brought on suitable forms, avoiding numerical ill-conditioned formulae. The purely non-linear part of the wave making procedure becomes integrated in the fully non-linear formulation. The ease in implementation and efficiency in use make pneumatic wave makers a good choice for further investigations of many different wave phenomenae.

A novel wave damping procedure is outlined. The main point is to damp the (scaled) tangential velocity at the free surface. For this purpose, an additional term is introduced in the Bernoulli equation at the free surface, namely the term given in Eq. (22). A modified dynamic boundary condition becomes $\tilde{\phi}_t + \nabla^{-1}\cdot(\gamma\nabla\tilde{\phi}) + g\eta + \frac{1}{2}\tilde{\boldsymbol{u}}\cdot\nabla\tilde{\phi} - \frac{1}{2}\tilde{v}V = B(t)$, where the practical evaluation of the ∇^{-1} operator is specified in Eq. (23) of the paper. We note that the horizontal gradient of this equation yields $\nabla\tilde{\phi}_t + \gamma\nabla\tilde{\phi} + \nabla[g\eta + \frac{1}{2}\tilde{\boldsymbol{u}}\cdot\nabla\tilde{\phi} - \frac{1}{2}\tilde{v}V] = 0$. The latter equation illustrates the main point of working with a damping coefficient γ, that varies in the space coordinate, appearing in front of the $\nabla\tilde{\phi}$ term, damping the physical tangential velocity at the free surface. The γ is a non-zero (smooth) function in regions where damping is required, but is zero in the wave propagation domain.

Axisymmetric outwards propagating waves, produced by an axisymmetric oscillating pressure, are tested with two different damping beaches. One is axisymmetric (see Fig. 1) and one is complex (see Fig. 3(a)). The simulations show that all the energy of the outgoing waves are absorbed by the present damper. Damping of a steep solitary wave, including damping of the mass, exhibits a complete absorption of the wave energy. Neither wave reflection nor emission are observed. Damping of waves due to advancing pressure distributions are efficient as well.

The implementation of this absorber in any existing numerical tank is rather trivial. The main advantage is that all kinds of waves are efficiently damped. The damping has the same strength for all wavelengths. No a priori knowledge of the wave field is needed for an efficient procedure.

Acknowledgments

This work was conducted under the Strategic University Programme 'Modelling of currents and wave for sea structures' and the BmatA-progamme 'Computational methods for stratified flows involving internal waves', both funded by the Research Council of Norway.

References

[1] B. Alpert, L. Greengard, T. Hagstrom, J. Comput. Phys. 180 (1) (2002) 270–296.
[2] B. Büchmann, P. Ferrand, J. Skourup, Run-up on a body in waves and current. Fully nonlinear and finite-order calculations, Appl. Ocean Res. 22 (2000) 349–360.
[3] B. Büchmann, J. Skourup, K.F. Cheung, Run-up on a structure due to second-order waves and a current in a numerical tank, Appl. Ocean Res. 20 (1998) 297–308.
[4] D. Clamond, J. Grue. Dynamics of the transient leading part of a wave train, in: T. Miloh, G. Zilman (Eds.), Faculty of Engineering, Tel Aviv University, Proceedings of the 15th International Workshop on Water Waves and Floating Bodies, Caesarea, Israel, 2000, pp. 28–31.
[5] D. Clamond, J. Grue, A fast method for fully nonlinear water wave computations, J. Fluid Mech. 447 (2001) 337–355.
[6] R.G. Dean, R.A. Dalrymple, Water wave mechanics for engineers and scientists, Adv. Series Ocean Eng. 2 (1991).
[7] D. Fructus, D. Clamond, J. Grue, Ø. Kristiansen, An efficient model for three-dimensional surface wave simulations. Part I: Free space problems. J. Comput. Phys. (2005) to appear.
[8] J. Grue, On four higly nonlinear phenomenae in wave theory and marine hydrodynamics, Appl. Ocean Res. 24 (2002) 261–274.
[9] D. Givoli, Review article: Non-reflective boundary conditions, J. Comput. Phys. 94 (1) (1991) 1–29.
[10] D. Givoli, High-order local non-reflecting boundary conditions: a review, Wave Motion 39 (4) (2004) 319–326.
[11] M. Israeli, S. Orszag, Approximation of radiation boundary conditions, J. Comput. Phys. 41 (1981) 115–135.
[12] J.E. Romate, Absorbing boundary conditions for free surface waves, J. Comput. Phys. 99 (1) (1992) 135–145.
[13] J.V. Wehausen, E.V. Laitone, Surface waves, Handbuch der Physik 9 (3) (1960) 446–778.